An ab Initio and Raman Investigation of Magnesium(II) Hydration

Cory C. Pye*

Department of Chemistry, The University of Calgary, Calgary, Alberta, Canada T2N 1N4

W. W. Rudolph

TU Dresden, Institute of Virology, University Hospital, Gerichtsstrasse 5, D-01069 Dresden, Germany

Received: June 22, 1998; In Final Form: August 21, 1998

The weak polarized Raman band assigned to the ν_1-MgO_6 mode of the hexaaquo Mg(II) ion has been studied over the temperature range 25 to 125 °C. The 356 cm^{-1} stretching mode frequency decreases by about 3 cm^{-1} but broadens by 13 cm^{-1} over a 100 °C temperature range. A depolarized mode at 235 cm^{-1} could be assigned to ν_2. These data suggest that the hexaaquo Mg(II) ion is thermodynamically stable in perchlorate and chloride solutions. In sulfate solutions, an equilibrium exists between the hexaaquo ion and an inner-sphere sulfato complex. Ab initio geometry optimizations of $Mg(H_2O)_6^{2+}$ were carried out at the Hartree−Fock and Møller−Plesset levels of theory, using various basis sets up to 6-31+G*. Frequency calculations confirm that the T_h structure is a minimum. The unscaled frequencies of the MgO_6 unit are lower than the experimental frequencies, and scaling only marginally improves the agreement. The theoretical binding enthalpy for the hexaaquo Mg(II) ion accounts for about 70% of the experimental hydration energy of Mg(II). A comparison of three models for the second hydration sphere is presented, and the most suitable is found to be one of lower symmetry *T*, in which alternate faces of the MgO_6 octahedron are H-bonded to water trimers. The unscaled Hartree−Fock frequencies agree very well with our experimental observations, giving nearly exact agreement with experiment.

1. Introduction

The structure of aqueous metal ions has been of considerable interest to chemists studying the properties of solutions. In the past decade or two, much computational effort has been expended in order to define predominant species in aqueous solution. Theoretical calculations have proven to be a valuable tool in understanding the complex behavior of electrolyte solutions.

In addition to theoretical methods, Raman spectroscopy has been extensively used to elucidate the spectroscopic characteristics of hydrated cations in aqueous solutions. However the strong quasi-elastic Rayleigh wing, extending over 500 cm^{-1}, prohibits the clear detection of the weak low-frequency modes of the metal aquo ions.[1,2] Although difference spectroscopy or the subtraction of a synthetic background can be employed, the fact that anions alter the low-frequency Raman spectrum of water[3] places some doubt on the validity of the subtraction procedure, as previously pointed out.[4−7] The use of reduced spectra, constructed by normalizing the low-frequency Raman data for the Bose−Einstein temperature factor (*B*) and a frequency factor, as in eq 1, gives accurate relative intensity data.[8,9]

$$R_Q(\bar{\nu}) = I(\bar{\nu})\cdot(\bar{\nu}_0 - \bar{\nu}_i)^{-4}\cdot\bar{\nu}_i\cdot B \qquad (1)$$

An ion in water may be regarded as being a series of concentric shells of water molecules, where the successive shells become more and more weakly bound to the shell preceding it until the interaction becomes indistinguishable from bulk water. Diffraction experiments clearly indicate the oscillations associated with the shell concept, giving the average distances between the metal ion and its solvation spheres.[10]

Magnesium(II) ions, possessing a high charge-to-radius ratio, are strongly hydrated in aqueous solutions. A hexahydrate has been established by both proton NMR in 3−4 M aqueous perchlorate at low temperatures[11] (−70 °C) and by X-ray diffraction,[12] who found an internuclear Mg−O distance of 2.11 Å. The exchange of water at 25 °C (which gives us an indication of kinetic stability) has been found to proceed at a rate of 5.3×10^5 and gives the thermodynamic parameters $\Delta H^\dagger = 42.7$ kJ mol^{-1}, $\Delta S^\dagger = 8$ J mol^{-1} K^{-1}.[13]

Earlier vibrational studies on aquo complexes, including Mg(II), may be found in refs 14 and 15. The temperature dependence of Raman band parameters was measured by Bulmer, Irish, and Ödberg,[16] who observed the totally symmetric vibration of the hydrated Mg(II) in nitrate solutions from −32 to 99 °C and found that ν_1 splits into two band components at 362 and 343 cm^{-1} as the temperature increases. Several possible explanations were given. A weakening of the hydration sphere, permitting entry of more water molecules into the first hydration sphere seems unlikely because entropy should favor a lower coordination number as the temperature is increased. The second argument, a distortion of octahedral symmetry, is even less likely. A third argument suggests that the hydration sphere is perturbed by nitrate at higher temperatures, but no diagnostic splitting of the ν_4 nitrate band was observed. However, in solutions more concentrated than 2 M, evidence for contact ion pair formation was found.[17] A complete study of the temperature dependence is warranted for nitrate systems but is outside

* Corresponding author.

10.1021/jp982709m CCC: $15.00
Published on Web 11/05/1998

the scope of the present work. However, we will present evidence for contact ion pairing in the analogous sulfate systems.

In our previous work, we presented combined Raman spectroscopic and ab initio investigations of lithium[4,5] and cadmium ions.[6,7] We present here our initial investigation of magnesium(II), including the second hydration sphere, as alluded to in these papers. We also would like to highlight some difficulties inherent in the computational study of these systems.

We also present Raman spectra of magnesium perchlorate and magnesium chloride solutions as a function of concentration and temperature, in order to draw conclusions about the thermodynamic stability of the hexaaquo complex. Since perchlorate does not penetrate the first hydration sphere, the hexaaquomagnesium species can be vibrationally characterized. Furthermore, quantitative intensity measurements of the totally symmetric stretching mode was carried out. The aim of measuring the Raman spectra is to characterize the Mg(II) ion with vibrational spectroscopy and try to answer the open question about the stability of the Mg(II) hexaaquo ion at elevated temperatures. Finally, $MgSO_4$ solutions were studied over a broad concentration and temperature range, in order to obtain information about the sulfato complex formation and its effect on the Raman modes of $Mg-OH_2$ and the ligated sulfate itself.

2. Experimental Details, Data Analysis, and Computational Methodology

A 3.00 mol/kg $Mg(ClO_4)_2$ stock solution was prepared in order to characterize the MgO_6 modes. The solution was prepared by weight from $Mg(ClO_4)_2$ (Fisher) and an appropriate amount of double-distilled water. The solution was analyzed for magnesium by colorimetric titration with standard EDTA.[18] The pH of the stock solution was found to be 6.26. A 3.30 mol/kg $MgCl_2$ stock solution was prepared from $MgCl_2 \cdot 6H_2O$ (Fisher) and distilled water by weight as well as a 3.015 mol/kg $MgSO_4$ stock solution (pH = 5.95) from $MgSO_4 \cdot 7H_2O$ (Fisher). Solution densities were determined with a pycnometer (5 mL) at 25 °C.

A deuterated solution was prepared by dissolving the $Mg(ClO_4)_2$ in D_2O (Cambridge Isotope Laboratories, 99.9%). The deuteration grade, checked by Raman spectroscopy, (in the OD and OH region) was better than 99.5%. The solutions were filtered through a 0.22 μm Millipore filter into a 150 mm i.d. quartz tube. Raman spectra were obtained with a Coderg PHO Raman spectrometer using the 488.0 nm argon ion laser line with a power level at the sample of about 0.9 W. The slit widths of the double monochromator were set normally at 1.8 cm^{-1}. The Raman scattered light was detected with a PMT cooled to −20 °C, integrated with a photon counter and processed with a boxcar averager interfaced to a personal computer. Two data points were collected per wavenumber. To increase the signal-to-noise ratio, six data sets were collected for each scattering geometry ($I_{||}$ and $I_{\perp}$). A quarter wave plate before the slit served to compensate for grating preference. $I_{||}$ and $I_{\perp}$ spectra were obtained with fixed polarization of the laser beam by changing the polaroid film at 90° between the sample and the entrance slit to give the scattering geometries:

$$I_{||} = I(Y[ZZ]X) = 45\alpha'^2 + 4\beta'^2 \quad (2)$$

$$I_{\perp} = I(Y[ZY]X) = 3\beta'^2 \quad (3)$$

A computer program was applied that corrected the measured intensity for the fourth-power frequency factor and then set the lowest data point to zero and the highest to 999 on a relative scale. In addition, corrections were made for the Bose-Einstein temperature factor, $B = [1 - \exp(-hc\bar{\nu}/kT)]$ and the frequency factor, $\bar{\nu}$, to give the reduced, or R, spectrum. The I and R spectra are different only in the low-frequency region.

Further spectroscopic details about the high-temperature measurement, the band fit procedure, and details about R normalized Raman spectra are described in previous publications.[19−22]

For quantitative measurements, the perchlorate band, ν_1-ClO_4^- at 935 cm^{-1} was used as an internal standard. For this purpose a $MgCl_2$ solution with NH_4ClO_4 was prepared by weight from $MgCl_2 \cdot 6H_2O$, NH_4ClO_4, and doubly distilled water. Three different stock solutions were prepared, namely, stock solution no. I (2.3361 M in $MgCl_2$ and 0.2738 M NH_4ClO_4), stock solution no. II (2.4870 M in $MgCl_2$ and 0.1257 M NH_4ClO_4), and stock solution no. III (2.8878 M in $MgCl_2$ and 0.2478 M NH_4ClO_4). From the R_{iso} spectra, the relative isotropic scattering coefficient $S(\nu_1\text{-}MgO_6)$ was obtained. The use of S values has the advantage that relative scattering coefficients can be put on an absolute scale if an absolute standard reference is considered. For further details about S values cf. ref 20.

$MgCl_2$ solution spectra, 5.90 and 3.48 mol/kg, were measured with a Raman and IR spectrometer at the Mining Academy Freiberg (Saxony). The apparatus was described in detail in ref 19.

Ab initio Hartree−Fock calculations with the STO-3G,[23] 3-21G,[24] and 6-31G*[25] basis sets were employed. Gaussian 92[26] was used for all calculations. All structures were confirmed to be minima (except where otherwise noted) via analytic frequency calculation. A diffuse sp-shell was added to the oxygen to give the standard 6-31+G* basis set[27] (no diffuse functions were added to magnesium since the cationic nature of magnesium renders them unnecessary). Møller−Plesset perturbation theory (with frozen cores) was used to approximate correlation effects (as MP2/6-31G* and MP2/6-31+G*).

3. Results and Discussion

3.1. Raman Spectra of $Mg(ClO_4)_2$, $MgCl_2$, and $MgCl_2$ plus NH_4ClO_4 Solutions. *3.1.1. $Mg(ClO_4)_2$.* The overall Raman spectrum of an aqueous $Mg(ClO_4)_2$ solution was analyzed between 70 and 1200 cm^{-1}. The free ClO_4^- ion possesses T_d symmetry and has nine modes of internal vibrations spanning the representation $\Gamma_{vib} = a_1 + e + 2f_2$. All modes of vibration are Raman active, but only the f_2 modes are IR active. A spectrum of a 3.00 mol/kg $Mg(ClO_4)_2$ solution shows the predicted four Raman-active bands for the tetrahedral ClO_4^-. The $\nu_1(a_1)$-ClO_4^- band, centered at 934 cm^{-1}, is totally polarized, with $\rho = 0.006$ (the asymmetry on the low-frequency side at 924 cm^{-1} is due to Fermi resonance of the overtone of the ν_2(e)-ClO_4^- bending mode, which occurs at 464 cm^{-1}, with the fundamental $\nu_1(a_1)$) whereas $\nu_3(f_2)$-ClO_4^-, centered at 1114 cm^{-1}, is depolarized, as are the deformation modes $\nu_4(f_2)$-ClO_4^- at 631 cm^{-1} and ν_2(e)-ClO_4^- at 464 cm^{-1}.

The Raman spectra of the $Mg(ClO_4)_2$ solution were measured at three different temperatures in the wavenumber range from 70 to 800 cm^{-1}. In addition to the ClO_4^- bending modes, two additional bands are observed. The band at 356 ± 1 cm^{-1} (fwhh = 50 cm^{-1}) is almost completely polarized (ρ ca. 0.01). In addition to this mode, a very weak broad band centered at 180 ± 10 cm^{-1} is also visible. A band around 190 cm^{-1} is also seen in pure water and is moderately intense but slightly polarized. This band has been assigned as a restricted translation

TABLE 1: Temperature Dependence of the ν_1 MgO_6 Band Parameters in a 3.30 mol/kg Aqueous $MgCl_2$ Solution

T (°C)	peak max (cm^{-1})	fwhh (cm^{-1})
25	356	45
80	354	52
120	353	58

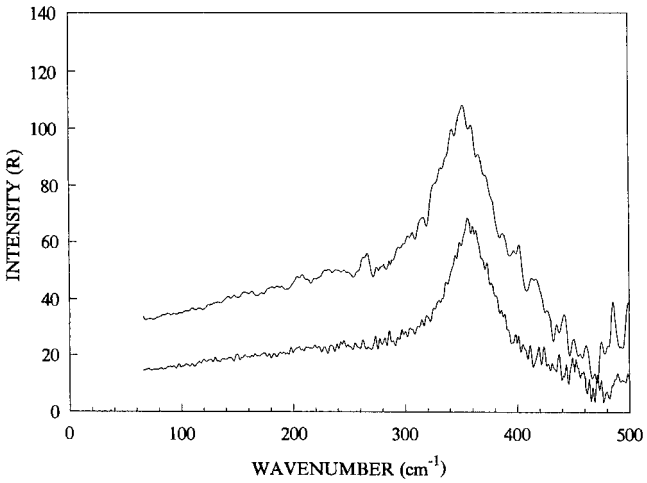

Figure 1. R_{iso} Raman spectra of a 3.00 *m* $Mg(ClO_4)_2$ solution in the wavenumber range from 60 to 500 cm^{-1} at 25 and 125 °C.

mode of the H-bonded water molecules, and the band is anion and concentration dependent (refs 8, 9). In concentrated $Mg(ClO_4)_2$ solutions other H-bonds are important, namely, OH···OCl O_3^-. The intensity of the band arising from this H-bond is very weak in the isotropic spectrum, and, because of the weakness of the H-bond, the intermolecular H-bond stretching mode does not shift to a higher frequency than the analogous band in pure water.

The polarized band at 356 cm^{-1} is due to the Mg^{2+}−oxygen symmetric stretching mode of the $[Mg(OH_2)_6]^{2+}$ cation, $\nu_1(a_{1g})$-MgO_6. The vibrational modes of the MgO_6 unit possess O_h symmetry under the assumption that the water molecules are treated as point masses. This assumption is certainly sufficient enough in aqueous solutions. The 15 normal modes of the MgO_6 unit span the representation $\Gamma_{vib}(O_h) = a_{1g} + e_g + 2f_{1u} + f_{2g} + f_{2u}$. The modes $\nu_1(a_{1g})$ (polarized) and $\nu_2(e_g)$ and $\nu_5(f_{2g})$ (both depolarized) are Raman active, the modes $\nu_3(f_{1u})$ and $\nu_4(f_{1u})$ are IR active, but the mode $\nu_6(f_{2u})$ is not observable in solution spectra. The frequency of $\nu_1(a_{1g})$-MgO_6 does not show a significant shift with increasing temperature, but the half-width increases. Furthermore, the band symmetry persists, indicating that the perchlorate does not penetrate into the inner sphere of the water molecules. The frequencies and half-width for the symmetric stretch of the magnesium hexaaquo complex (ν_1-MgO_6) as a function of temperature are given in Table 1. The R spectra of a 2.00 mol/kg $Mg(ClO_4)_2$ at 25 and 125 °C are presented in Figure 1. These Raman spectroscopic results show, clearly, that over the applied temperatures the hexaaquo complex remains stable, in contrast to the sulfate system, in which a sulfate−water exchange is taking place.[19]

3.1.2. $MgCl_2$. Furthermore, $MgCl_2$ solutions (5.90 and 3.48 mol/kg at 25 °C) were measured in the wavenumber region 200−4000 cm^{-1} (Mining Academy, Freiberg). The results confirm the existence of the symmetric stretching mode of $Mg(OH_2)_6^{2+}$ obtained in perchlorate solutions ($\nu_1(a_{1g})$-MgO_6 = 356 cm^{-1}). A depolarized mode at 235 cm-1 could be assigned to $\nu_5(f_{2g})$. In the infrared spectrum $\nu_3(f_{1u})$ was observed at 420 cm^{-1}. Nakagawa and Shimanouchi[15] found $\nu_3(f_{1u})$ surprisingly low (310 cm^{-1} for $MgSO_4 \cdot 7H_2O$) compared to the solution value. Inspection of the published IR crystal spectrum,[15] however, shows a weak mode at ca. 400 cm^{-1}. This finding is supported by the ab initio molecular orbital calculations as described in the next section. The Raman active mode $\nu_2(e_g)$ is too weak to be observed. The IR active mode $\nu_4(f_{1u})$ could also not be detected. The vibrational spectroscopic frequency values are quite different and support the centrosymmetric symmetry for the MgO_6 unit.

For low-frequency vibrations the excitation of "hot bands" must be considered. At the lowest temperature investigated 12% of the molecules occupy the $v = 1$ level of ν_1, and this fraction increases about 22% over the temperature range. Thus transitions $2 \leftarrow 1$ must be contributing to the observed band profile. The small 3 cm^{-1} shift to lower frequencies of the band maximum may arise from these transitions, but the anharmonicity of the potential surface cannot be large. The temperature dependence of the fwhh was explained in ref 7.

In the $MgCl_2-D_2O$ system, this band is observable at 339 cm^{-1} in accordance with the expected isotope shift:

$$\nu_1[(Mg(OD_2)_6^{2+}] = \sqrt{18.02/20.03} \cdot \nu_1[(Mg(OH_2)_6^{2+}] = 0.948 \cdot 356\ cm^{-1} = 339\ cm^{-1} \quad (4)$$

3.1.3. $MgCl_2-NH_4ClO_4$. Relative intensity measurements for three different $MgCl_2$ solutions as a function of concentration (see Experimental section) yield a relative scattering coefficient for the ν_1 Mg−O mode, $S_h = 0.0077$. The perchlorate band, $\nu_1(a_1)$-ClO_4^- at 935 cm^{-1}, served as the reference band. The S_h value is defined as the corrected relative scattering efficiency of the $[M(OH_2)_n]^{m+}$ aqueous metal hydrates in ref 2 (it should be noted that the S_h values in ref 8 are compared to $\nu_1(a_1)$-NO_3^- and are taken as percentage). Furthermore S_h is defined in the pure isotropic R spectrum. The S_h value for ν_1-MgO_6 is very small and reflects the fact that between Mg and O the electron density is not very high, or, in the language of inorganic chemistry, the bond is mostly ionic. However, with transition metal hexaaquo ions, a S_h value of 0.032 for the ν_1-Zn−O mode[21] was found, for ν_1-Cd−O a value of 0.045 was found,[7] and for ν_1-Hg−O a value of 0.143.[28] This reflects the increase in the softness of these group IIb metal ions with increase in the periodic number.

As a summary, these Raman spectroscopic data show clearly that over the applied temperature range the hexaaquo complex remains stable. However, in the Mg sulfate solution, a water−ligand exchange takes place and Mg−sulfato complexes are formed.

3.2. Raman Spectra of $MgSO_4$ Solutions. *3.2.1. $(NH_4)_2SO_4$.* To facilitate the interpretation of the magnesium sulfate spectra, a summary of previous studies by one of us[20,29,30] of the sulfate bands observed in ammonium sulfate solutions is given. This system may be taken as a model "free" sulfate system, which we then compare to the $MgSO_4$ system.

The free SO_4^{2-} ion, like ClO_4^-, possesses T_d symmetry and has nine modes of internal vibrations spanning the representation $\Gamma_{vib} = a_1 + e + 2f_2$. All modes of vibration are Raman active, but only the f_2 modes are IR active. An overview spectrum of a 3 mol/kg $(NH_4)_2SO_4$ solution (Figure 2) shows the predicted four Raman-active bands. The $\nu_1(a_1)$ band, centered at 981.4 cm^{-1}, is totally polarized, whereas $\nu_3(f_2)$, centered at 1110 cm^{-1}, and the deformation modes $\nu_4(f_2)$ at 617 cm^{-1} and $\nu_2(e)$ at 452 cm^{-1}, are depolarized. The ν_1 band remains symmetrical up to 200 °C, but the Gauss-Lorentz shape factor changes. The broad weak band at 190 cm^{-1} is due to intermolecular vibrations,

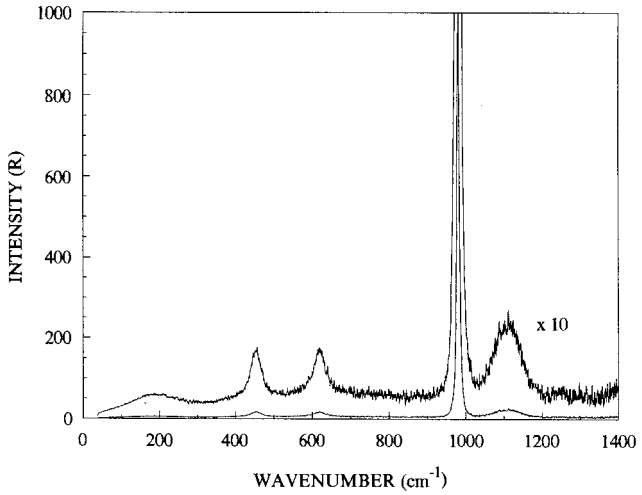

Figure 2. Overview Raman spectrum (R_{iso}) of a 3.00 *m* $(NH_4)_2$ SO_4 solution at 25 °C.

specifically the restricted translational mode of a hydrogen-bonded water dimer.

3.2.2. $MgSO_4$. The Raman spectra of $MgSO_4$ solutions show additional features besides the "free" SO_4^{2-} modes, described above, and a mode for the hexaaquo cation at 354 ± 2 cm^{-1} (which is downshifted ca. 2 cm^{-1} compared to the ν_1-MgO_6 mode in perchlorate solutions, and broadened). If sulfate is ligated directly to Mg(II), replacing one water molecule in the inner sphere (monodentate), the vibrational features of the coordinated sulfate should change as well as the $Mg(OH_2)_{6-n}$ (n = coordination number of ligand) modes of the remaining water molecules. Furthermore, a Mg(II)−ligand mode should be observed at low frequencies (200−300 cm^{-1}). At first the low-frequency region of $MgSO_4$ solution will be discussed and then the sulfate stretching region.

3.3.2.a. The Low-Frequency Region (40−600 cm^{-1}). The most significant differences between the $(NH_4)_2SO_4$ solution and $MgSO_4$ solution spectra occur in the low-frequency region. In Figure 3a the polarized Raman spectra (R-format) of a 3.015 mol/kg $MgSO_4$ solution at 25 and 120 °C are compared with a 3.00 mol/kg $(NH_4)_2$ SO_4 solution at 25 °C in the wavenumber range from 40 to 800 cm^{-1}. The need for spectra in R-format is evident by comparing parts b and c of Figure 3, where the latter includes the broad quasi-elastic Rayleigh wing. In addition to the deformation modes of sulfate ν_4 at 617 cm^{-1}, ν_2 at 452 cm^{-1}, and the restricted translational mode at 190 cm^{-1}, in the spectra of $MgSO_4$ solution the polarized mode, ν_1-MgO_6 at 354 cm^{-1}, is noticeable, as already mentioned. The deformation modes of sulfate are broadened, and this broadening increases with temperature. Furthermore, a polarized mode at 245 cm^{-1} and a shoulder at 330 cm^{-1} on the low-frequency side of ν_1-MgO_6 is detectable. Again, these features are more pronounced at elevated temperatures. These spectroscopic features are more evident in Figure 3b, in which polarized, depolarized and the constructed isotropic spectrum (R-format) of a 3.015 mol/kg $MgSO_4$ solution are presented. The bending modes ν_4-SO_4^{2-} and ν_2-SO_4^{2-}, which are broader in $MgSO_4$ solution spectra than in $(NH_4)_2SO_4$ solution spectra, show very weak contributions in the isotropic spectra at 490 ± 10 cm^{-1} and 645 ± 5 cm^{-1}, well apart from the frequencies normally observed in the anisotropic spectrum (452 and 617 cm^{-1}).

Furthermore, in Figures 4a,b, Raman spectra in R_{iso} format of a 3.00 mol/kg $Mg(ClO_4)_2$ solution with a 3.015 mol/kg $MgSO_4$ solution are presented in the wavenumber range from 40 to 500 cm^{-1} at 25 and 125/120 °C. A shoulder at ca. 330

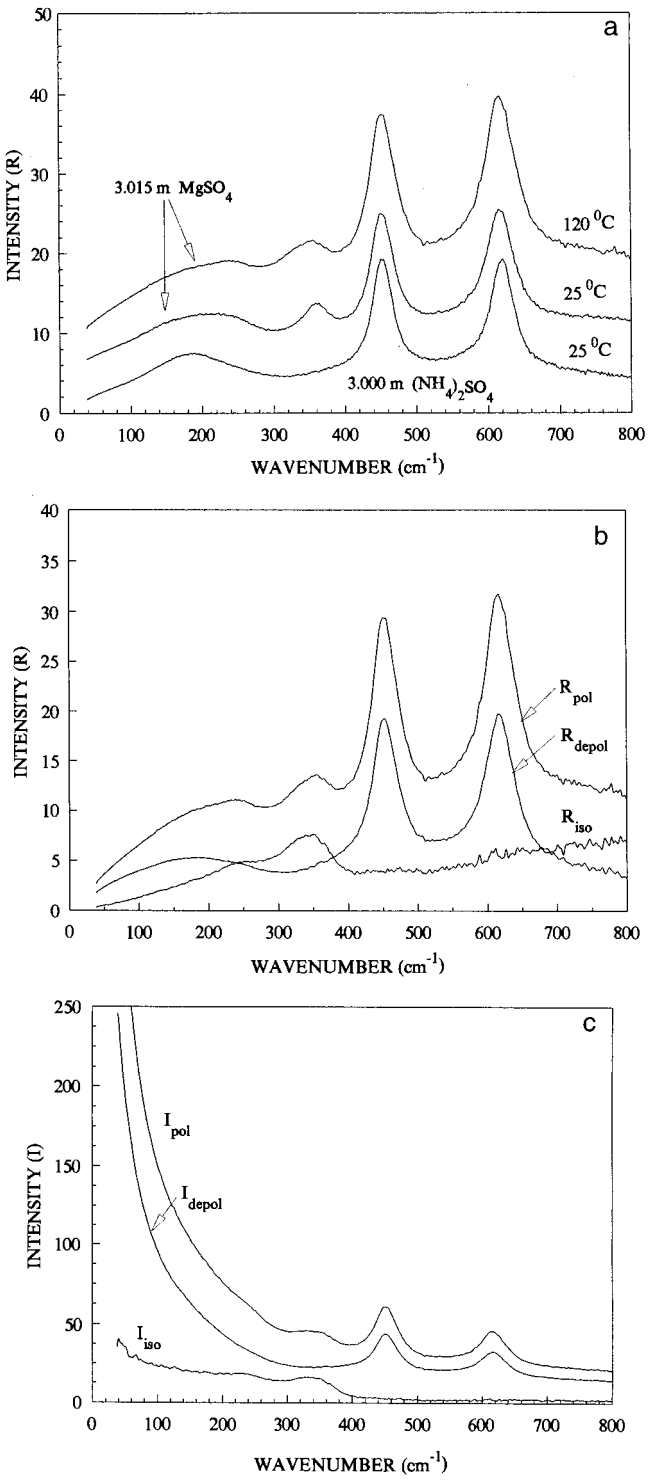

Figure 3. (a) R_{pol} Raman spectra of a 3.015 *m* $MgSO_4$ solution at 25 and 120 °C (top, center) and of a 3.00 *m* $(NH_4)_2$ SO_4 solution at 25 °C (bottom), in the wavenumber range from 40 to 800 cm^{-1}. (b) R_{iso}, R_{pol}, and R_{depol} Raman spectra of a 3.015 *m* $MgSO_4$ solution at 120 °C in the wavenumber range from 40 to 800 cm^{-1}. (c) I_{iso}, I_{pol}, and I_{depol} Raman spectra of a 3.015 *m* $MgSO_4$ solution at 120 °C in the wavenumber range from 40 to 800 cm^{-1}.

cm^{-1} on the low-frequency side of ν_1-MgO_6 is more pronounced at 120 °C. At 120 °C the whole band is shifted to 348 ± 2 cm^{-1}. An isotropic component at 245 cm^{-1}, also temperature dependent, is clearly observable in the $MgSO_4$ solution.

The shoulder at 330 cm^{-1} is most likely due to the Mg−OH_2 mode of the Mg−sulfato complex (inner-sphere ion pair), $[Mg(OH_2)_5$ $OSO_3]$. The penetration of the sulfate into the first

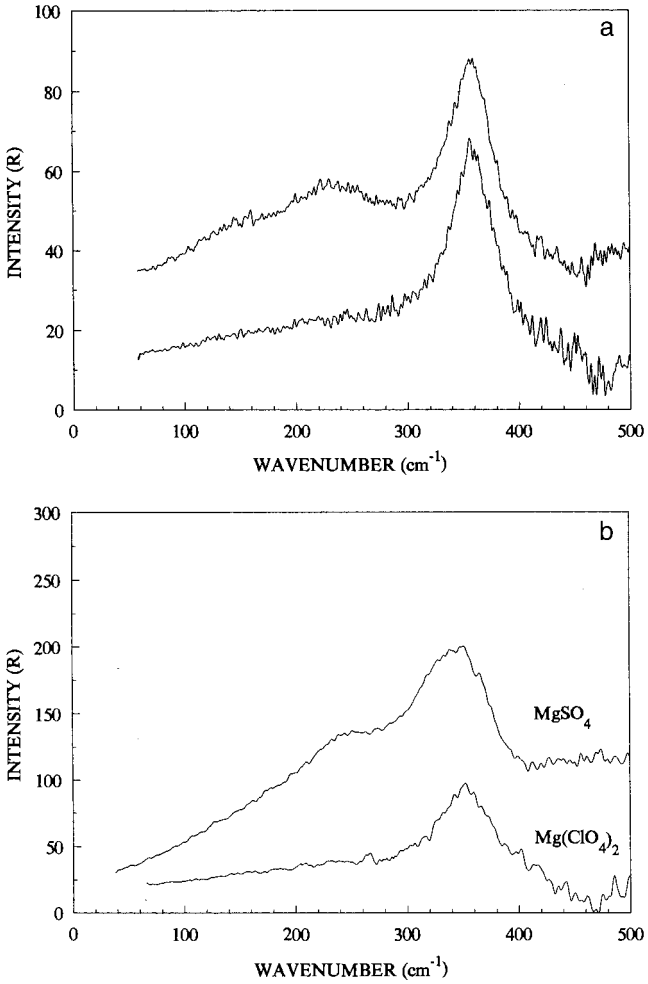

Figure 4. (a) R_{iso} Raman spectra of 3.015 *m* $MgSO_4$ and 3.00 *m* $Mg(ClO_4)_2$ solutions in the wavenumber range from 40 to 500 cm^{-1} at 25 °C. (b) R_{iso} Raman spectra of 3.015 *m* $MgSO_4$ (120 °C) and 3.00 *m* $Mg(ClO_4)_2$ (125 °C) solutions in the wavenumber range from 40 to 500 cm^{-1}.

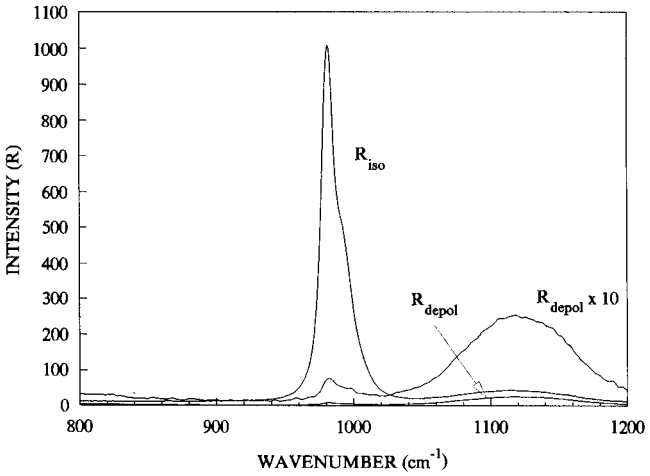

Figure 5. R_{iso} and R_{depol} Raman spectra of a 3.015 *m* $MgSO_4$ solution at 120 °C in the wavenumber range from 800 to 1200 cm^{-1}.

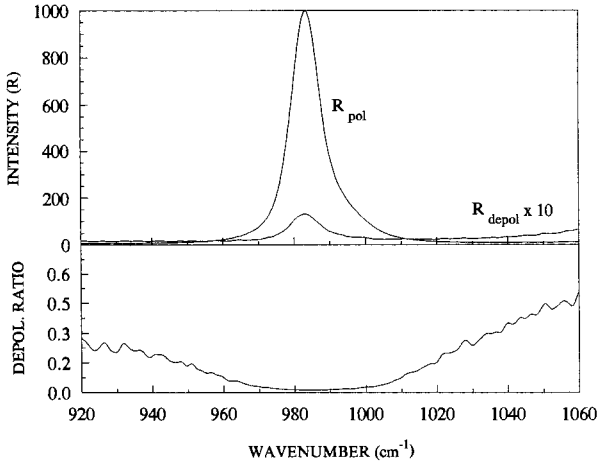

Figure 6. R_{pol} and R_{depol} Raman spectra of a 3.015 *m* $MgSO_4$ solution at 25 °C in the wavenumber range from 920 to 1060 cm^{-1} and, additionally, the depolarization ration as a function of wavenunmber.

coordination sphere reduces the octahedral symmetry of the hexaaquo complex, leading to a shift of the symmetric stretch of Mg−OH_2 and a pronounced low-frequency asymmetry at 330 cm^{-1}. A splitting of the symmetric stretch of the aquo complex cannot be observed because the bands are too broad and overlap. The strongest argument for the direct contact of SO_4^{2-} with Mg^{2+} stems from the Mg−O ligand vibration at 245 cm^{-1}.

3.2.2.b. Sulfate Stretching Mode Region (800−1300 cm^{-1}). The low-frequency region is crucial for assigning the Mg^{2+}−sulfato complex as an inner-sphere complex as well as attributing the high-frequency component at 993 cm^{-1} to this ion pair. The ν_1-SO_4^{2-} band centered at 983.3 ± 0.2 cm^{-1} exhibits a high-frequency component at 993 cm^{-1}. Figure 5 presents the Raman spectra of a 3.015 mol/kg $MgSO_4$ solution at 120 °C in the sulfate stretching region, and Figure 6 presents the same solution at 25° along with the depolarization ratio. Clearly, the two sulfate components of the ν_1-SO_4^{2-} mode at 979 and 992 cm^{-1} are observable, as well as the very broad ν_3-SO_4^{2-} at 1120 cm^{-1}. The component band at 993 cm^{-1} is temperature and concentration dependent. In Figure 7, the R_{iso} spectra of a 0.571 mol/kg $MgSO_4$ solution in the wavenumber region from 920 to 1060 cm^{-1} at four different temperatures are presented. At 25 °C the 993 cm^{-1} component is only visible as a shoulder while at 198 °C two separate bands are observable. At −10 °C the intensity of the high-frequency shoulder, is almost completely reduced in intensity compared with the band at 25 °C. With decreasing $MgSO_4$ concentration, the component at 993 cm^{-1} disappears at a concentration of ca. 0.05 mol/kg as demonstrated in Figure 8. Curve-resolution into three components via least-squares fitting results in an intense band centered at 983 cm^{-1} and a less intense band at the high-frequency side at 993 cm^{-1} and, additionally, a very small band at 967 cm^{-1} arising from $S^{18}O/^{16}O_3^{2-}$ (the intensity of this band is constant and, as expected, according to its fixed natural abundance, 0.81%). The high-frequency component of ν_1-SO_4^{2-} at 993 cm^{-1} is insensitive to deuteration and is also observable in a $MgSO_4/D_2O$ solution.

A more quantitative analysis of the ion pairing in $MgSO_4$ solutions will be given in a later publication.[28]

3.3. Computation. The previous section gave experimental evidence for a discrete MgO_6 unit in aqueous solution by direct observation of a band that is assigned to the totally symmetric stretch of this unit. We present independent computational support for this assignment, including a comparison of several different cluster models and theoretical levels. We also present a compilation of previous experimental and theoretical work related to this study.

3.3.1. The Hexaaquo Complex. In Table 2, we give (instead of presenting again) a compilation of calculated literature Mg−O distances and binding enthalpies of the $Mg(H_2O)_6^{2+}$ species,

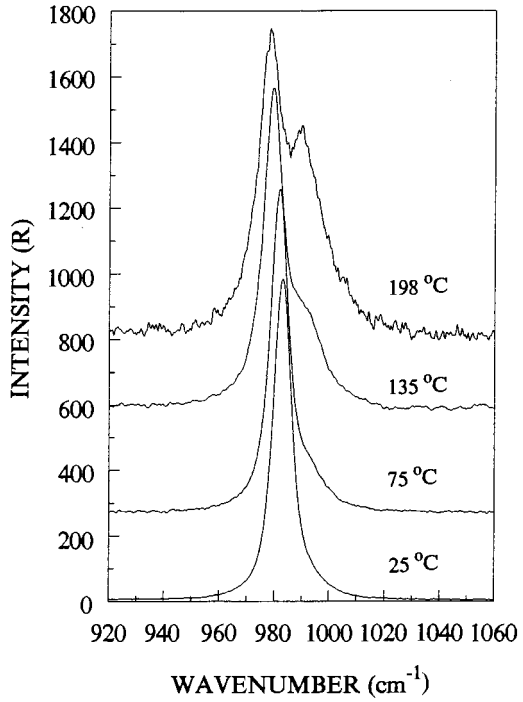

Figure 7. R_{iso} Raman spectra of a 0.571 *m* $MgSO_4$ solution at four different temperatures (25, 75, 135, and 198 °C) in the wavenumber range from 920 to 1060 cm^{-1}.

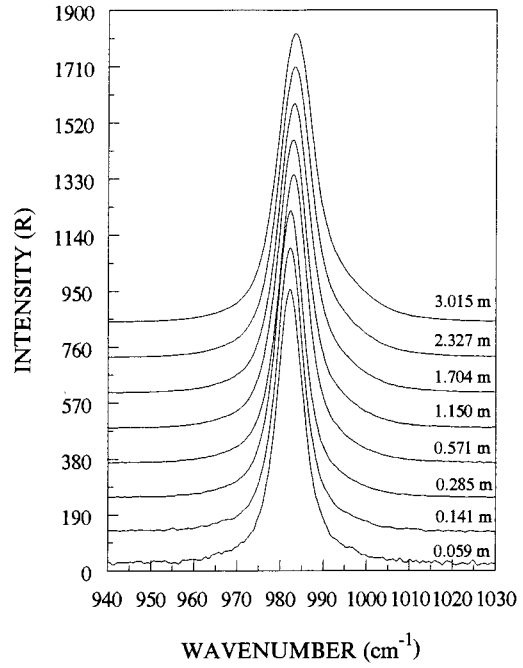

Figure 8. R_{iso} Raman spectra of $MgSO_4$ solution at 25 °C as a function of molar concentration in the wavenumber range from 940 to 1030 cm^{-1}.

whose structure is given in Figure 9. From these data it is clear that minimal basis sets underestimate the experimental solution Mg−O distance[49] of 2.09 Å. Using basis sets of double-ζ or better quality generally gives similar results for the Mg−O distances. Our results (Table 3) confirm some of these literature data and also show the insensitivity of the Mg−O distance to the effect of correlation. The slight difference (0.004 Å) between our present results and those of ref 45 are due to the effect of core correlation. Our results with the "full" HF/6-31+G* basis set showed very minor Mg−O differences in the 0.0001 Å region, demonstrating that diffuse functions on the metal are not necessary for geometry optimization. All minimum energy structures possessed T_h symmetry. Our best calculated result is in excellent agreement with experiment.

TABLE 2: A Compilation of Literature Data for $Mg(H_2O)_6^{2+}$

ref	Mg−O (Å)	$-E_{int}$ (kJ/mol)	level
32	2.01	1484	CNDO
33, 34	2.12	1740	2-body (HF+CI)
		1693	2-body (SZ) 4/4 + Barthelat pseudopotential
		1571	2-body (SZCP) counterpoise
		1823	2-body (DZP)
		1477	3-body (HF+CI)
		1368	3-body (SZ)
		1273	3-body (SZCP)
		1298	3-body (DZP)
35	1.932	1950	STO-3G
36	2.05		6-21G
37	2.099	1581	6-31G
	2.084	1348	DZP
38		1513	DZ
		1333	DZ+O(d)
		1327	DZP
		1318	DZP+O(d)
40	2.102	1367	TZP
39	2.050		3-21G(*)
	2.082	1458	3-21G(*) + solvent (Born-767 kJ/mol)
41	2.084		DZP
42	2.062		DZP
43	2.097	1473	MP2−FULL/6-31G*
44	2.10	1359	MP2/CEP-31G
45	2.105		HF/6-31G
		1240	MP2−FC/6-31G*
		1243	MP4SDQ-FC/6-31G*
		1161	MP2/6-311++G**
	2.107	1246	MP2−FULL/6-31G*
		1161	MP2/6-311++G**
		1155	MP2/6-311++G(2d,p)
46	2.109	1280	HF/6-31+G*
		1275	MP2/6-31+G*
47	2.10	1363	HF/TZ2P
48	2.08	1271	B3LYP/6-311+G(2d,2p)//B3LYP/LANL2DZ

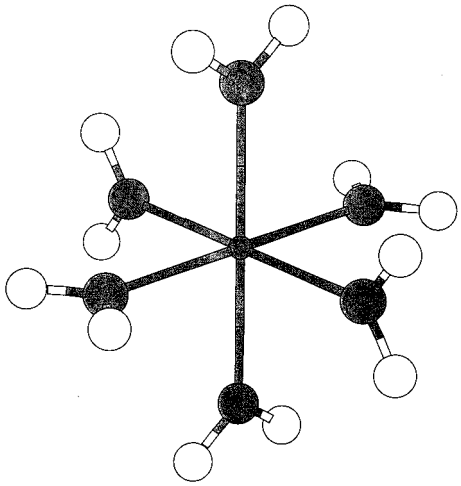

Figure 9. Structure model for $Mg(H_2O)_6^{2+}$.

The unscaled frequencies are given in Table 4. We note that the addition of diffuse functions generally makes a greater difference to the calculated IR and Raman intensities than the calculated frequencies. At the Hartree−Fock level, the water twisting frequencies are increased by about 20 cm^{-1}. For frequencies above about 400 cm^{-1}, the MP2 frequencies are uniformly lower than the corresponding Hartree−Fock values.

It is clear that the calculated ν_1 frequency of $[Mg(OH_2)_6]^{2+}$ is underestimated relative to experiment at all of the calculated

TABLE 3: Optimized Geometries of $Mg(H_2O)_6^{2+}$

level	Mg−O (Å)	O−H (Å)	HOH (deg)	−*E* (hartrees)	E_{bind} (kJ/mol)	ΔH_{bind}^{298} (kJ/mol)
HF/STO-3G	1.931	0.979	104.8	647.056 984	−1968.20	−1912.01
HF/3-21G	2.043	0.968	109.8	651.916 574	−1871.19	−1816.73
HF/6-31G*	2.105	0.954	107.0	655.423 833	−1436.80	−1394.72
MP2-FC/6-31G*	2.103	0.975	106.2	656.570 997	−1517.03	−1476.30
HF/6-31+G*	2.109	0.954	107.0	655.438 430	−1364.91	−1322.00
MP2-FC/6-31+G*	2.109	0.977	106.2	656.607 322	−1408.73	−1366.79

TABLE 4: Unscaled Calculated $Mg(H_2O)_6^{2+}$ Frequencies (in cm^{-1}) and Intensities; $\Gamma_{vib} = 3a_g(R, tp) + a_u(na) + 3e_g(R, dp) + e_u(na) + 5f_g(R, dp) + 8f_u(IR)$[a]

		HF/6-31G*		HF/6-31+G*		MP2/6-31G*		MP2/6-31+G*	
mode	sym	ν	I[b]	ν	I	ν	I	ν	I
δ-OMgO	F_u	99.9	4.20	102.0	3.00	94.6	7.00	98.2	6.49
δ-OMgO	F_g	128.3	0.00	133.5	0.00	106.9		111.3	
δ-OMgO	F_u	163.3	0.91	163.2	1.11	151.9	3.30	151.5	4.01
τ-HOH	E_u	222.0		244.7		225.8		227.5	
ν-MgO	E_g	262.2	0.16	256.8	0.12	272.8		267.3	
τ-HOH	F_g	290.9	1.96	312.6	0.67	287.9		295.8	
ν-MgO	A_g	327.5	0.35	323.5	0.49	329.3		324.0	
ω-HOH	F_u	392.9	38.5	388.7	9.24	380.5	345	390.4	167
ω-HOH	F_g	417.7	3.81	434.9	2.25	375.7		395.4	
τ-HOH	A_u	428.4		453.2		430.0		456.1	
ν-MgO	F_u	453.1	392	465.7	379	419.8	105	421.8	259
ρ-HOH	F_g	582.4	0.19	582.0	0.02	546.1		549.2	
ρ-HOH	F_u	608.6	636	608.5	631	578.1	535	582.5	500
δ-HOH	F_u	1831.3	322	1827.7	342	1727.1	281	1716.9	317
δ-HOH	E_g	1831.4	7.36	1828.1	3.84	1726.6		1717.5	
δ-HOH	A_g	1837.6	0.43	1834.3	0.08	1733.6		1723.4	
ν_s-OH	E_g	4017.2	38.7	4006.4	33.0	3742.2		3702.4	
ν_s-OH	F_u	4019.5	306	4008.4	279	3743.6	253	3703.0	216
ν_s-OH	A_g	4029.7	247	4017.5	293	3751.0		3708.2	
ν_{as}-OH	F_g	4104.5	60.6	4096.9	46.6	3840.9		3806.5	
ν_{as}-OH	F_u	4105.2	508	4097.6	503	3841.3	421	3806.9	431

[a] R = Raman active with tp = totally polarized and dp = depolarized; IR = infrared active; na = not active. [b] Either the IR activities (km/mol) or Raman intensities ($Å^4$/au) are given (the mutual exclusion rule ensures that the mode cannot be active in both the IR and Raman spectra). No MP2 Raman intensities were calculated.

levels, in some cases by up to 32 cm^{-1} (9%). This disagreement is not due to a deficiency of the theoretical level but arises from a deficiency of the cluster model used to calculate the frequencies. The six water molecules represent only the first hydration shell. In solution these water molecules form strong hydrogen bonds with the water molecules in the second hydration shell because of the polarizing effect of the magnesium ion. Our earlier studies of lithium[4,5] and cadmium[6,7] support this view, because including several second sphere waters raises the ν_1 frequency to more closely match experiment. Other metal aquo complexes exhibit the same behavior, namely, Be^{2+}, Zn^{2+}, Al^{3+}, Sc^{3+}, Ga^{3+}, and In^{3+}.[50]

One has two options when correcting for this cluster deficiency. The more computationally demanding one is to explicitly include the second solvation shell when calculating the frequencies. This is discussed later in the text. The less demanding alternative is to *scale* the frequencies for the effect of the second solvation sphere. The scaled frequencies (to match ν_1), along with selected experimental frequencies, is given in Table 6. Scale factors of 1.085, 1.099, 1.082, and 1.099 were determined for the HF/6-31G*, HF/6-31+G*, MP2/6-31G*, and MP2/6-31+G* levels, respectively. Other scaling methods have been considered previously for the related cadmium analog.[20] A compilation of experimental values for various magnesium-containing species is given in Table 5. The bands ν_4 and ν_6 have not been observed experimentally. We must note the deviation between the calculated and experimental ν_3.[15] This suggests to us that the assignment of the mode at 310 cm^{-1} is incorrect. We observe this mode at 420 cm^{-1}. We also note the disagreement between the predicted and observed ν_5 and (recently reassigned) ν_3 modes, which no reasonable scale factor can eliminate. For the ν_3 mode, accounting for correlation effects decreases the frequency by 30−40 cm^{-1}, whereas the effect is not as large for the other modes.

For Mg^{2+}, the experimental ΔG_{hyd}^{298} is −1838 kJ/mol and the ΔG_{hyd}^{298} is −1931 kJ/mol (taken from Table 5.10 of ref 49, p 107). Our best value for the gas-phase binding enthalpy of six water molecules is about 70% of the hydration enthalpy. Since the ab initio calculation considers the waters as being in the gas phase, we must correct for the phase transition from liquid to gas (57.2 kJ/mol at 25°) in order to compare with the hydration enthalpy. Our best corrected value becomes −1023 kJ/mol, which reduces the percentage to 53%. This demonstrates that although the majority of the hydration energy occurs from binding of the first solvation shell, a sizable portion is still unaccounted for, which suggests that a second hydration sphere should improve the agreement considerably.

3.3.2. The Octadecaaquo Complex. The symmetry of the hexaaquo complex is T_h. It is therefore reasonable to assume that there exist structures of T_h symmetry formed by adding a water molecule in such a way as to H-bond to the hydrogens of the first hydration sphere, forming a second hydration sphere. Each of the water molecules of the first sphere defines a local plane coinciding with a plane of symmetry of the entire hexaaquo complex. There are two possible ways of maintaining this high symmetry. The second-sphere water can either be embedded in this plane (A, see Figure 10) or, alternatively, be bisected by this plane (B, see Figure 11). Our initial expectations were that the latter would be preferred because a wagging

TABLE 5: Experimentally Observed Skeleton Modes of MgO_6 (in O_h Symmetry)

ref	species	$\nu_1(a_{1g})$	$\nu_2(e_g)$	$\nu_3(f_{1u})$	$\nu_5(f_{2g})$
51, 52	Mg^{2+} + {Cl^-,NO_3^-, ClO_3^-}, sat.	376			
53	$MgSO_4 \cdot 7H_2O$	382			
	$Mg(NO_3)_2$, 3N	380			
	$MgCl_2$	376			
54, 55	$MgSO_4 \cdot 7H_2O$	370	258		205
56	$K_2Mg(SO_4)_2 \cdot 6H_2O$	374			
	$MgSO_4 \cdot 7H_2O$	366			
57	$(NH_4)_2Mg(SO_4)_2 \cdot 6H_2O$	365			
15	$MgSO_4 \cdot 7H_2O$			310	
58	$MgSO_4 \cdot 7H_2O$			320	
59	$Mg(NO_3)_2$, sat.	370			
	$MgSO_4$, sat.	360			
	$Mg(ClO_4)_2$, sat.	360			
60	$Mg(NO_3)_2$, 7.6 N	365	315		240
	$Mg(NO_3)_2$, 1.9 N	365			
	$MgSO_4$, 5.2 N	365			240
	$MgSO_4$, 1.5 N	365			
	$MgCl_2$, 7.2 N	361	315		240
	$MgCl_2$, 3.7 N	363			240
	$MgCl_2$, 1.4 N	360			
	$MgCl_2$, 4.2 N D_2O	344	302		240
61	$Mg(NO_3)_2$ 90 °C, $R = 77$	363			
	$R = 42$	356			
	$R = 20$	354			
62	$Mg(NO_3)_2$ 25 °C	357			240
	$Mg(NO_3)_2 \cdot 6H_2O$ melt, 98 °C	345			240
63	$Mg(NO_3)_2 \cdot 6H_2O$	362	312		222
	$Mg(NO_3)_2 \cdot 6D_2O$	344	300		208
16	$Mg(NO_3)_2$, 3.06 m, −32 °C	363			
	−4 °C	361			
	26 °C	359			
	52 °C	357			
	79 °C	355			
	80 °C	355			
	99 °C	355			
	25 °C, 1.02 m	359			
	25 °C, 4.36 m	358			

TABLE 6: MgO_6 Skeleton Modes (in O_h Symmetry). Experimental Frequencies and Calculated Frequencies (Scaled) in Aqueous $Mg(ClO_4)_2$ Solution

		Scaled Frequencies (cm^{-1})			
assignment and activity	exptl freq (cm^{-1})	HF/ 6-31G*	HF/ 6-31+G*	MP2/ 6-31G*	MP2/ 6-31+G*
$\nu_1(a_{1g})$ Ra	356[a]	356	356	356	356
$\nu_2(e_g)$ Ra	315[b]	284	282	295	293
$\nu_3(f_{1u})$ IR	420[c]	492	512	454	464
$\nu_4(f_{1u})$ IR		177	179	163	167
$\nu_5(f_{2g})$ Ra	240[b]	139	146	114	122
$\nu_6(f_{2u})$ na		109	112	102	108

[a] Isotropic Raman frequency. [b] Depolarized, as measured in $Mg(NO_3)_2$ solutions. See ref 60. [c] IR frequency.

motion of the waters may more favorably orient the lone pair of the second-sphere oxygen toward the hydrogen, as in the case of the water dimer.[64] At the HF/3-21G level, structure A is preferred (total energies in a.u. (3-21G): A, −1559.401 705; B, −1559.358 386), whereas at the HF/6-31G* level, a slight preference for B is established (A, −1567.834 331; B, −1567.834 433). At the latter level, the Mg−O distances for structures A and B are 2.082 and 2.083 Å, respectively, and the H-bond distance is 1.8894 and 1.9256 Å, respectively. *However, neither of these structures represent an energy minimum.* Desymmetrization along the highest frequency mode destroys the inversion center and reduces the symmetry to point group *T*, but the energy is lowered substantially. Physically, adjacent faces of the MgO_6 become inequivalent, but alternate

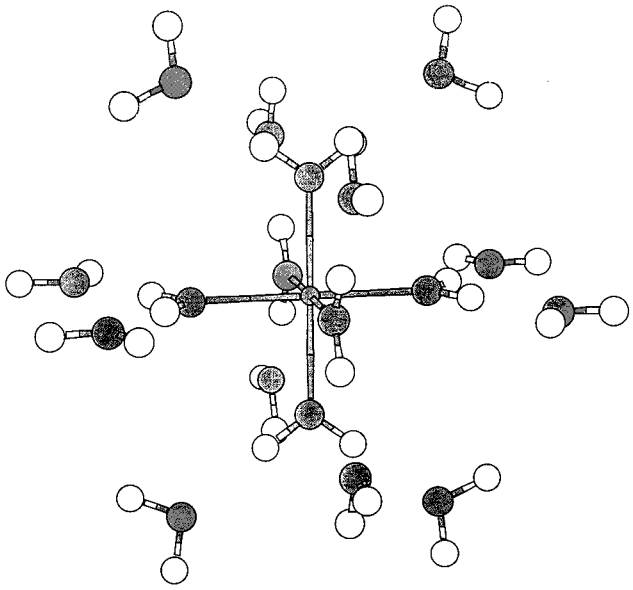

Figure 10. Structure model A for $Mg(H_2O)_{18}^{2+}$.

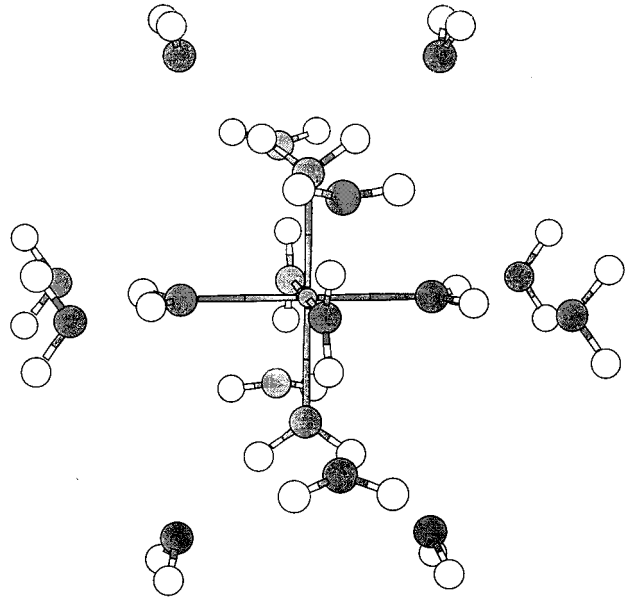

Figure 11. Structure model B for $Mg(H_2O)_{18}^{2+}$.

faces retain their symmetric relationship and thus the three waters on the edges of each alternate face cluster together.

The resulting structure C is given in Figure 12, with the geometry data given in Table 7. The waters cluster together to form cyclic water trimers internally hydrogen-bonded to each other (locally, of C_3 symmetry), as well as forming strong hydrogen bonds to the inner sphere. This structure does not possess any imaginary frequencies and is therefore a minimum-energy structure. Our results call into question the structure of Siegbahn and co-workers[48] (which corresponds to our structure B). Although they used the sophisticated B3LYP density functional method to obtain the geometry, which includes the correlation energy, only a double-ζ basis set was used. Our basis set included polarization functions, which are known to be necessary to represent the anisotropy in the density (in both traditional ab initio approaches and density functional methods), as evidenced by both the carbon−oxygen distances and dipole moments in ref 65.

The frequencies of the $MgAq_{18}^{2+}$ cluster are given in Table 8. In some cases, the MgO_6 modes couple strongly with either

TABLE 7: Structural Parameters, Energy (hartrees), and Thermodynamic Parameters (ΔE, Binding Energy, at 0 K and ΔH, Enthalpy of Cluster Formation, at 298.15 K) Calculated for the $Mg(H_2O)_{18}^{2+}$ Cluster, Denoted Mg[6+12]

	HF/3-21G	HF/6-31G*	HF/6-31+G*
bond length (in Å)			
Mg−O (first water sphere)	2.0359	2.0889	2.0930
Mg−O (second water sphere)	4.1107	4.3155	4.3477
O−H (first water sphere)	0.9745	0.9572	0.9570
O−H(A) (second water sphere)	0.9657	0.9501	0.9505
O−H(B) (second water sphere)	0.9829	0.9555	0.9553
HO1···H bond length	1.7673	1.9306	1.9521
angle θ (deg)			
HOH angle (first water sphere)	113.00	109.00	108.72
HOH angle (second water sphere)	112.03	107.08	107.25
energy (hartree)	−1559.514301	−1567.888963	−1567.957558
E_{bind} (0 K) (kJ/mol)	−3357.77	−2319.42	−2168.86
ΔH^{298} (kJ/mol)	−3162.90	−2171.27	−2021.64

TABLE 8: Unscaled HF/6-31G* Frequencies (cm^{-1}) of Octadecaaquomagnesium(II); $\Gamma_{vib} = 13A + 13E + 40F$

frequency	symmetry	mode	frequency	symmetry	mode
31.9	F	$(H_2O)_3$ twist	544.1	A	H_2O (2) lib.
38.1	E	$(H_2O)_3$ trans.	593.8	F	H_2O (1) wag
47.9	F	$(H_2O)_3$ trans	629.9	F	H_2O (1) twist
48.6	A	$(H_2O)_3$ twist	630.0	E	H_2O (1) twist
61.9	F	$(H_2O)_3$ rock	654.5	A	H_2O (1) twist
96.3	F	MgO_6 def. + $(H_2O)_3$ rock	722.2	F	H_2O (1) wag
112.9	F	MgO_6 def. + $(H_2O)_3$ rock	770.3	F	H_2O (1) rock
119.7	E	$(H_2O)_3$ rock	816.6	F	H_2O (2) lib.
138.6	F	$(H_2O)_3$ rock	828.0	A	H_2O (2) lib.
143.3	A	$(H_2O)_3$···MgO_6 str. sym.	858.0	F	H_2O (1) rock
149.7	F	$(H_2O)_3$ H-bond str. asym.	1824.2	F	HOH bending outer-sph.
169.9	F	$(H_2O)_3$ H-bond str. asym.	1824.8	E	HOH bending outer-sph.
175.6	E	$(H_2O)_3$ H-bond str. asym.	1825.9	F	HOH bending outer-sph.
191.2	F	$(H_2O)_3$ H-bond str. sym.	1833.8	A	HOH bending outer-sph.
194.7	A	$(H_2O)_3$ H-bond str. sym.	1834.7	F	HOH bending outer-sph.
201.5	F	MgO_6 def.	1869.9	E	HOH bending inner-sph.
246.2	F	MgO_6 def.	1875.5	F	HOH bending inner-sph.
263.5	F	MgO_6 def. + H_2O (2) lib.	1891.0	A	HOH bending inner-sph.
301.1	E	MgO_6 str. + H_2O (2) lib.	3920.1	E	OH str. sym. inner-sph.
315.8	F	H_2O (2) lib.	3928.2	F	OH str. sym. inner-sph.
323.0	F	H_2O (2) lib.	3956.2	A	OH str. sym. inner-sph. + sym. outer-sph.
333.9	E	MgO_6 str. + H O (2) lib.	3962.0	F	OH str. asym. inner-sph. + sym. outer-sph.
355.7	A	MgO_6 str.	3967.8	A	OH str. sym. inner-sph. + sym. outer-sph.
363.3	F	H_2O (2) lib.	3974.2	F	OH str. asym. inner-sph. + sym. outer-sph.
385.5	A	H_2O (2) lib.	3996.5	F	OH str. asym. inner-sph. + sym. outer-sph.
414.0	F	H_2O (2) lib.	4005.0	E	OH str. sym. outer-sph.
428.4	F	H_2O (2) lib.	4019.7	F	OH str. asym. inner-sph. + sym. outer-sph.
434.5	E	H_2O (2) lib.	4023.4	F	OH str. asym. inner-sph. + sym. outer-sph.
449.1	F	MgO_6 str.	4126.9	F	OH. str. asym. outer-sph.
481.2	F	H_2O (2) lib.	4127.6	F	OH. str. asym. outer-sph.
500.1	F	H_2O (2) lib.	4127.6	E	OH. str. asym. outer-sph.
515.1	E	H_2O (2) lib.	4129.0	F	OH. str. asym. outer-sph.
518.7	F	H_2O (2) lib.	4129.6	A	OH. str. asym. outer-sph.

second-sphere water librations or restricted translational modes. In a real solution, because of hydrogen bonding between the second hydration sphere and the bulk solution, the symmetry-allowed coupling would not be as severe. In any case, the modes that may be unambiguously assigned are the ν_1 and ν_3 stretching modes at 356 and 449 cm^{-1} and the deformation modes at 202 and 246 cm^{-1}. We may average the two e-modes, which consist partially of Mg−O stretching, to obtain a frequency of 317 cm^{-1}. We clearly see that the experimental frequencies, with the exception of ν_3, are predicted, without scaling, to an accuracy of 10 cm^{-1}. Adding correlation should have the same effect on the ν_3 mode in both the hexa and octadeca models, decreasing this value by 30 cm^{-1} for this basis set, giving a corrected ν_3 of about 420 cm^{-1}, in good agreement with our observed IR result.[28]

Since the second-sphere waters occur as trimers, the restricted translational modes of the individual waters group together as the twisting, rocking, and translational motions perpendicular and parallel to the trimer-metal axis, and within each trimer we see asymmetric and symmetric H-bond stretches. The symmetric H-bond stretch, calculated to be at 195 cm^{-1}, is observed experimentally at 190 cm^{-1} in pure water.[11]

The water bending modes shift to higher frequencies, from 1595 cm^{-1} in the gas phase to 1636 cm^{-1} in bulk water and to 1650 cm^{-1} in magnesium hexaaquo complex.[62] The 55 cm^{-1} difference between gas phase and hexaaquo ion is underestimated in the hexaaquo model we initially used, where shifts of 11, 37, −2, and 42 cm^{-1} are given at the HF/6-31G*, HF/6-31+G*, MP2/6-31G*, and MP2/6-31+G* levels, respectively. The octadecaaquo model predicts the shift correctly at HF/6-31G*, giving a change in frequency of 64 cm^{-1}, which when scaled by an optimal scale factor of 0.8730 for the water bending mode at HF/6-31G* gives 56 cm^{-1}.

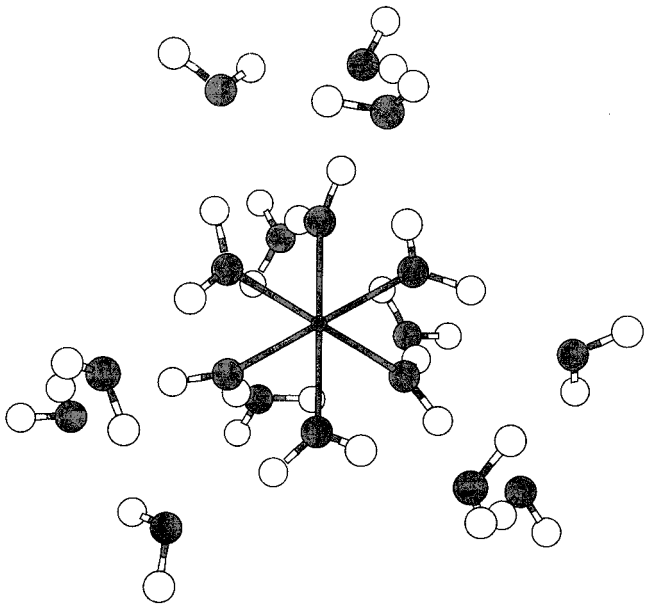

Figure 12. Structure model C for $Mg(H_2O)_{18}^{2+}$.

TABLE 9: Predicted Geometry and Energies for Water Dimer

	O···H length (Å)	$-E$ (hartrees)	E_{bind} kJ/mol	ΔH^{298} kJ/mol
HF/STO-3G	1.750	149.941 244	−24.79	−15.27
HF/3-21G	1.825	151.189 404	−45.90	−36.64
HF/6-31G*	2.026	152.030 456	−23.53	−16.24
HF/6-31+G*	2.014	152.044 059	−22.51	−14.94
MP2/6-31G*	1.959	152.405 356	−30.60	−23.08
MP2/6-31+G*	1.930	152.430 722	−29.30	−21.38

The unscaled OH stretching modes are predicted to lie about 100 and 170 cm^{-1} lower than the gas-phase values for the symmetric and asymmetric stretching vibrations, respectively.

The binding enthalpies of the octadecaaquo complex are given in Table 7. At the Hartree−Fock level, the binding energy slightly overestimates the hydration enthalpy. With the phase correction mentioned earlier, the value drops to −992 kJ/mol (cf. −978.80 kJ/mol for the hexaaquo complex at the same level). One of the reasons why there is so little improvement may be that the Hartree−Fock method underestimates the water−water interaction relative to more sophisticated calculations such as MP2. This hypothesis was disproved by calculating the dimerization energies, as shown in Table 9. Since the experimental binding energy (D_e) is 22.8 ± 2.1, in excellent agreement with the Hartree−Fock values, the discrepancy must lie elsewhere. It is possible that other structures may be favored in solution or that the second hydration sphere (if it exists) possesses a different number of water molecules which maximize stabilizing interactions. Notwithstanding this, it is clear that at least the structures and frequencies are reproduced well with this octadecaaquo complex, which is our main interest.

4. Conclusions

The Raman spectrum of magnesium perchlorate and chloride solutions show a band at 356 cm^{-1} attributable to the symmetric stretching mode of the hexaaquo cation $Mg(H_2O)_6^{2+}$ and is stable over a wide temperature range. The weak intensity of this mode is consistent with the ionic nature of the Mg−O bond. In magnesium sulfate solutions, two new modes at 245 and 330 cm^{-1} appear and are more pronounced at higher temperatures. New sulfate modes appear at 490, 645, 993, and 1120 cm^{-1}. These changes suggest that a contact ion pair between magnesium and sulfate ion can be formed and is in a temperature-dependent equilibrium with free sulfate and the hexaaquomagnesium ion.

Theoretical calculations on the hexaaquomagnesium ion reproduce the structure reasonably well but underestimate the Mg−O stretching and deformation mode frequencies. Scaling the results to reproduce the ν_1 frequency gives only modest improvement. The calculated binding energy of the hexaaquo complex gives about 50% of the hydration enthalpy. Calculations on the octadecaaquo complex, where 12 second-sphere waters are hydrogen-bonded to the first sphere, reveal a desymmetrization to point group *T*, where alternate faces of the octahedron possess a water trimer. None of the T_h structures were energy minima. The calculated MgO_6 frequencies are in much better agreement with experiment.

Note Added in Proof. The phase-corrected binding energies are generally much lower than anticipated, especially for the octadecaaquo cluster. It is now clear that this is due to the difference between the *macroscopic* heat of vaporization of water and the *microscopic* binding energy of small water clusters (Marcus, Y. *Ion Solvation*; Wiley: Chichester, 1985; pp 25−27, Figure 2.2 and Equation 2.3). The enthalpy of hydration may be approximated as

$$\Delta H^{298}_{solv}(I) = \sum_{i=1}^{\infty}[\Delta H^{298}_{i-1,i}(I) - \Delta H^{298}_{i-1,i}(H_2O)]$$

$$\approx \sum_{i=1}^{n}[\Delta H^{298}_{i-1,i}(I) - \Delta H^{298}_{i-1,i}(H_2O)] + \Delta H^{solv}(I(H_2O)_n) - \Delta H^{solv}(H_2O)_n)$$

$$= \lambda_n[\Delta H^{298}_{0,n}(I) - \Delta H^{298}_{0,n}(H_2O)]$$

The finite approximation would need to include the long-range electrostatic interactions ΔH^{solv}, which we deliberately ignore so as to obtain a fraction λ_n of the hydration enthalpy (which we express as a percentage). However, the approximation implicit in our above discussion, $\Delta H^{298}_{0,n}(H_2O) = n \times \Delta H^{298}_{vap}(H_2O)$, is too severe for our purposes, as seen by the small phase-corrected binding energy for the octadecaaquo cluster. To do this properly, one would need to calculate the binding enthalpies of small water clusters, which is not a trivial problem because of the many possible metrical configurations available. For Mg (and other divalent ions), the close agreement between the binding energy of the octadecaaquo cluster and the experimental hydration energy suggests that the ΔH_{vap} and the Born term for the charged cluster approximately cancel.

Acknowledgment. The assistance of scholarships (PGSB, PDF) granted by NSERC Canada to C.C.P. is gratefully acknowledged. The authors thank the Computing and Communications Department, Memorial University of Newfoundland, for computer time with a special thanks to DEC for providing an Alpha server 4100. W.W.R. thanks Prof. M. H. Brooker for the use of his Raman spectrometer. Furthermore, a DAAD scholarship (1993−1995) should be acknowledged as it was during this period that the research was mostly conducted.

References and Notes

(1) Irish, D. E.; Brooker, M. H. In *Advances in Infrared and Raman Spectroscopy*; Clark, R. J. H., Hester, R. E., Eds.; Heyden: London, 1976; Vol. 2, pp 212−311.

(2) Brooker, M. H. in *The Chemical Physics of Solvation, Part B. Spectroscopy of Solvation*; Dogonadze, R. R., Kalman, E., Kornyshev, A. A., Ulstrup, J., Eds.; Elsevier: Netherlands, 1986; pp 119−187.
(3) (a) Walrafen, G. E. *J. Chem. Phys.* **1962**, *36*, 1035−1042. (b) *J. Chem. Phys.* **1966**, *44*, 1546−1558.
(4) Rudolph, W.; Brooker, M. H.; Pye, C. C. *J. Phys. Chem.* **1995**, *99*, 3793−3797.
(5) Pye, C. C.; Rudolph, W. W.; Poirier, R. A. *J. Phys. Chem.* **1996**, *100*, 601−605.
(6) Rudolph, W. W.; Pye, C. C. *Z. Phys. Chem. (Munich)*, in press.
(7) Rudolph, W. W.; Pye, C. C. *J. Phys. Chem. B* **1998**, *102*, 3564−3573.
(8) Brooker, M. H.; Faurskov Nielsen, O.; Praestgaard, E. *J. Raman. Spectrosc.* **1989**, *19*, 71−78.
(9) For a review, see: Faurskov Nielsen, O. *Annu. Rep. Prog. Chem. C. Phys. Chem.* **1997**, *93*, 57−99.
(10) Burgess, J. *Metal Ions in Solution*; Horwood: Chicester, 1978; Section 4.4.
(11) Matwiyoff, N. M.; Taube, H. *J. Am. Chem. Soc.* **1968**, *90*, 2796−2800.
(12) (a) Caminiti, R.; Licheri, G.; Piccaluga, G.; Pinna, G. *J. Appl. Crystallogr.* **1972**, *12*, 34−38; (b) *Chem. Phys. Lett.* **1979**, *61*, 45−49.
(13) Neely, J. W.; Connick, R. E. *J. Am. Chem. Soc.* **1970**, *92*, 3476−3478.
(14) Adams, D. M. *Metal−Ligand and Related Vibrations*; E. Arnold: London, 1966; p 256 and references therein.
(15) Nakagawa, I.; Shimanouchi, T. *Spectrochim. Acta* **1964**, *20*, 429−439.
(16) Bulmer, J. T.; Irish, D. E.; Ödberg, L. *Can. J. Chem.* **1975**, *53*, 3806−3811.
(17) James, D. W.; Carrick, M. T.; Frost, R. L. *J. Raman. Spectrosc.* **1982**, *13*, 115−119.
(18) Vogel, A. I. *A Text-Book of Quantitative Inorganic Analysis*, 3rd ed.; Longman: London, 1961.
(19) Rudolph, W.; Irmer, G. *J. Solution Chem.* **1994**, *23*, 663−684.
(20) Rudolph, W. *Z. Phys. Chem (Munich)* **1996**, *194*, 73−95.
(21) Rudolph, W.; Brooker, M. H.; Tremaine, P. R. *Z. Phys. Chem. (Munich)*, in press.
(22) Rudolph, W.; Brooker, M. H.; Tremaine, P. R. *J. Solution Chem.* **1997**, *26*, 757−777.
(23) (a) H, Li−F: Hehre, W. J.; Stewart R. F.; Pople, J. A. *J. Chem. Phys.* **1969**, *51*, 2657−2664. (b) He, Ne−Ar: Hehre, W. J.; Ditchfield, R.; Stewart, R. F.; Pople, J. A. *J. Chem. Phys.* **1970**, *52*, 2769−2773.
(24) (a) H−Ne: Binkley, J. S.; Pople, J. A.; Hehre, W. J. *J. Am. Chem. Soc.* **1980**, *102*, 939−947. (b) Na−Ar: Gordon, M. S.; Binkley, J. S.; Pople, J. A.; Pietro, W. J.; Hehre, W. J. *J. Am. Chem. Soc.* **1982**, *104*, 2797−2803.
(25) (a) C−F 6-31G: Hehre, W. J.; Ditchfield, R.; Pople, J. A. *J. Chem. Phys.* **1972**, *56*, 2257−2261. (b) Na−Ar: Francl, M. M.; Pietro, W. J.; Hehre, W. J.; Binkley, J. S.; Gordon, M. S.; Defrees, D. J.; Pople, J. A. *J. Chem. Phys.* **1982**, *77*, 3654−3665. (c) H, C−F polarization functions: Hariharan, P. C.; Pople, J. A. *Theor. Chim. Acta (Berlin)* **1973**, *28*, 213−222.
(26) Frisch, M. J.; Trucks, G. W.; Schlegel, H. B.; Gill, P. M. W.; Johnson, B. G.; Wong, M. W.; Foresman, J. B.; Robb, M. A.; Head-Gordon, M.; Replogle, E. S.; Gomperts, R.; Andres, J. L.; Raghavachari, K.; Binkley, J. S.; Gonzalez, C.; Martin, R. L.; Fox, D. J.; Defrees, D. J.; Baker, J.; Stewart, J. J. P.; Pople, J. A. *Gaussian 92/DFT*, Revision F.4; Gaussian, Inc.: Pittsburgh, PA, 1993.
(27) Chandrasekhar, J.; Andrade, J. G.; v. R. Schleyer, P. *J. Am. Chem. Soc.* **1981**, *103*, 5609−5612.
(28) Rudolph, W. Memorial University of Newfoundland, Department of Chemistry. Unpublished results, 1996.
(29) Rudolph, W. W. *J. Chem. Soc., Faraday Trans.* **1998**, *94*, 489−499.
(30) Rudolph, W. W. *Ber. Bunsen-Ges. Phys. Chem.* **1998**, *102*, 183−196.
(31) Rudolph, W. Manuscript in preparation.
(32) Tretyak, V. M.; Baranovskii, V. I.; Sizova, O. V.; Kozhevnikova, G. V. *Zh. Strukt. Khim.* **1978**, *19*, 594−599.
(33) Ortega-Blake, I.; Novaro, O.; Leś, A.; Rybak, S. *J. Chem. Phys.* **1982**, *76*, 5405−5413.
(34) Ortega-Blake, I.; Leś, A.; Rybak, S. *J. Theor. Biol.* **1983**, *104*, 571−590.
(35) Maynard, A. T.; Hiskey, R. G.; Pedersen, L. G.; Koehler, K. A. *J. Mol. Struct.: THEOCHEM* **1985**, *124*, 213−221.
(36) Newton, M. D.; Friedman, H. L. *J. Chem. Phys.* **1985**, *83*, 5210−5218.
(37) Probst, M. M. *Chem. Phys. Lett.* **1987**, *137*, 229−233.
(38) Krauss, M.; Stevens, W. J. *J. Am. Chem. Soc.* **1990**, *112*, 1460−1466.
(39) Sánchez Marcos, E.; Pappalardo, R. R.; Rinaldi, D. *J. Phys. Chem.* **1991**, *95*, 8928−8932.
(40) Klobukowski, M. *Can. J. Chem.* **1992**, *70*, 589−595.
(41) Probst, M. M.; Hermansson, K. *J. Chem. Phys.* **1992**, *98*, 8995−9004.
(42) Ramondo, F.; Bencivenni, L.; Rossi, V.; Caminiti, R. *J. Mol. Struct.: THEOCHEM*, **1992**, *277*, 185−211.
(43) Bock, C. W.; Kaufman, A.; Glusker, J. P. *Inorg. Chem.* **1994**, *33*, 419−427.
(44) Garmer, D. R.i; Gresh, N. *J. Am. Chem. Soc.* **1994**, *116*, 3556−3567.
(45) Markham, G. D.; Glusker, J. P.; Bock, C. L.; Trachtman, M.; Bock, C. W. *J. Phys. Chem.* **1996**, *100*, 3488−3497.
(46) Glendening, E. D.; Feller, D. *J. Phys. Chem.* **1996**, *100*, 4790−4797.
(47) Periole, X.; Allouche, D.; Daudey, J.-P.; Sanejouand, Y.-H. *J. Phys. Chem. B* **1997**, *101*, 5018−5025.
(48) Pavlov, M.; Siegbahn, P. E. M.; Sandstrom, M. *J. Phys. Chem. A* **1998**, *102*, 219−228.
(49) Marcus, Y. *Chem. Rev.* **1988**, *88*, 1475−1498.
(50) (a) Pye, C. C. Unpublished material. (b) Pye, C. C. Ph.D. Thesis, Department of Chemistry, Memorial University of Newfoundland, 1997, Section 3.3.
(51) Silveira, A. *Compt. Rend.* **1932**, *194*, 1336−1338.
(52) Silveira A.; Bauer, E. *Compt. Rend.* **1932**, *195*, 416−418.
(53) Mathieu, J.-P. *Compt. Rend.* **1950**, *231*, 896−897.
(54) Lafont, R. *Compt. Rend.* **1957**, *244*, 1481−1483.
(55) Lafont, R. *Ann. Phys. (Paris)* **1959**, *13−4*, 905−963.
(56) Ananthanarayanan, V. *Z. Phys.* **1961**, *163*, 144−157.
(57) Ananthanarayanan, V. *Z. Phys.* **1962**, *166*, 318−327.
(58) Kermarec, Y. *Compt. Rend.* **1964**, *258*, 5836−5838.
(59) Hester, R. E.; Plane, R. A. *Inorg. Chem.* **1964**, *3*, 768−769.
(60) Silveira, A.; Marques, M. A.; Marques, N. M. *Mol. Phys.* **1965**, *9*, 271−276.
(61) Peleg, M. *J. Phys. Chem.* **1972**, *76*, 1019−1025.
(62) Chang, T. G.; Irish, D. E. *J. Phys. Chem.* **1973**, *77*, 52−57.
(63) Chang, T. G.; Irish, D. E. *Can. J. Chem.* **1973**, *51*, 118−125.
(64) Generated but not published during the course of an independent investigation: Pye, C. C.; Poirier, R. A.; Yu, D.; Surján, P. *J. Mol. Struct.: THEOCHEM* **1994**, *307*, 239−259. See also: Pye, C. C. Ph.D. Thesis, Department of Chemistry, Memorial University of Newfoundland, 1997, Section 3.4.
(65) Godbout, N.; Salahub, D. R.; Andzelm, J.; Wimmer, E. *Can. J. Chem.* **1992**, *70*, 560−571.